REPORT DOCUMENTATION PAGE

Form Approved
OMB No. 0704-0188

1. REPORT DATE *(DD-MM-YYYY)*	2. REPORT TYPE	3. DATES COVERED *(From - To)*
13-07-2009	Technical Paper	

4. TITLE AND SUBTITLE

Thrust Augmentation in Solid Rocket Motors Using Beamed Microwave Energy

5a. CONTRACT NUMBER

5b. GRANT NUMBER

5c. PROGRAM ELEMENT NUMBER

6. AUTHOR(S)
Natalia E. Gimelshein & Sergey F. Gimelshein (ERC); Andrew Ketsdever (AFRL/RZSA)

5d. PROJECT NUMBER

5f. WORK UNIT NUMBER
50260542

7. PERFORMING ORGANIZATION NAME(S) AND ADDRESS(ES)

Air Force Research Laboratory (AFMC)
AFRL/RZSA
10 E. Saturn Blvd.
Edwards AFB CA 93524-7680

8. PERFORMING ORGANIZATION REPORT NUMBER

AFRL-RZ-ED-TP-2009-281

9. SPONSORING / MONITORING AGENCY NAME(S) AND ADDRESS(ES)

Air Force Research Laboratory (AFMC)
AFRL/RZS
5 Pollux Drive
Edwards AFB CA 93524-7048

10. SPONSOR/MONITOR'S ACRONYM(S)

11. SPONSOR/MONITOR'S NUMBER(S)
AFRL-RZ-ED-TP-2009-281

12. DISTRIBUTION / AVAILABILITY STATEMENT

Approved for public release; distribution unlimited (PA #09328).

13. SUPPLEMENTARY NOTES
For presentation at the 45th AIAA Joint Propulsion Conference & Exhibit, Denver, CO, 2-5 August 2009.

14. ABSTRACT

Feasibility of using beamed microwave energy to increase thrust of solid rocket motors during launch is analyzed. Coupling of microwave radiation with internal energies of micron-sized alumina particles and the successive transfer of internal energy of particles to thermal and then kinetic energy of gas is expected to be the main mechanism of thrust increase. A two-phase two-way coupled capability has been developed. For the gas phase, the capability applies an Eulerian approach based on the solution of the Navier-Stokes equations, and uses VAC code modified to include particle source terms. For the particle phase, a Lagrangian approach is used based on a particle tracker that incorporates the impact of the gas and microwave radiation. The developed numerical capability is applied to compute the nozzle flow for a Castor 120 type motor with and without the microwave radiation. High gas density and thus fast collisional relaxation result in highly efficient transfer of microwave energy the kinetic energy of the flow. The total thrust was found to increase by 1.5% for a 100 MW/m^2 beam, and 15% for a 1GW/m^2 beam.

15. SUBJECT TERMS

16. SECURITY CLASSIFICATION OF:			17. LIMITATION OF ABSTRACT	18. NUMBER OF PAGES	19a. NAME OF RESPONSIBLE PERSON
a. REPORT	b. ABSTRACT	c. THIS PAGE			Dr. Andrew Ketsdever
Unclassified	**Unclassified**	**Unclassified**	SAR	13	19b. TELEPHONE NUMBER *(include area code)* N/A

Thrust Augmentation in Solid Rocket Motors Using Beamed Microwave Energy

Natalia E. Gimelshein[1] and Sergey F. Gimelshein[1]
ERC, Inc., Edwards AFB, CA 93524

Andrew Ketsdever[2]
Air Force Research Laboratory, Edwards AFB, CA 93524

Feasibility of using beamed microwave energy to increase thrust of solid rocket motors during launch is analyzed. Coupling of microwave radiation with internal energies of micron-sized alumina particles and the successive transfer of internal energy of particles to thermal and then kinetic energy of gas is expected to be the main mechanism of thrust increase. A two-phase two-way coupled capability has been developed. For the gas phase, the capability applies an Eulerian approach based on the solution of the Navier-Stokes equations, and uses VAC code modified to include particle source terms. For the particle phase, a Lagrangian approach is used based on a particle tracker that incorporates the impact of the gas and microwave radiation. The developed numerical capability is applied to compute the nozzle flow for a Castor 120 type motor with and without the microwave radiation. High gas density and thus fast collisional relaxation result in highly efficient transfer of microwave energy the kinetic energy of the flow. The total thrust was found to increase by 1.5% for a 100 MW/m^2 beam, and 15% for a 1GW/m^2 beam.

Nomenclature

A_e	=	nozzle exit area
A_t	=	nozzle throat area
c	=	speed of light
C	=	heat capacity
C_{p_g}	=	gas specific heat
$C_{p_{part}}$	=	specific heat of particle species
d_{part}	=	alumina particle diameter
E	=	electric field
f	=	microwave radiation frequency
M	=	Mach number
n_{part}	=	particle number density
Pr	=	Prandtl number
Re	=	Reynolds number of particles
Δt	=	time step for particle tracking
T_g	=	gas temperature
T_{p_j}	=	individual particle temperature
$\vec{u}_g$	=	gas velocity
u_{gi}	=	*i*-th component of gas velocity
$\vec{u}_p$	=	particle velocity

[1] Consultant, AIAA Senior Member
[2] Program Manager, Advanced Concepts, Propulsion Directorate, AIAA Associate Fellow

u_{pi} = i-th component of particle velocity
v_{pi} = individual particle velocity
$\tan(\delta)$ = loss tangent
ε_0 = dielectric permittivity of free space
ε' = relative dielectric constant
$\varepsilon_0\varepsilon'$ = real part of the relative permittivity
γ = specific heat ratio
λ = gas heat conductivity
ν = gas viscosity
ω = angular frequency
ρ = material density
ρ_g = gas density
$\widetilde{\rho_p}$ = density of particle species

I. Introduction

BEAMED energy propulsion is a technique which utilizes electromagnetic radiation from a remote source to increase the energy of a propellant. The electromagnetic radiation, in general, can originate from any source, although the most recent concepts feature either high power laser beams or microwaves. One significant advantage of beamed energy propulsion is that it requires no additional mass to be carried on-board the vehicle. Beamed energy propulsion can also overcome the inherent limitations on specific impulse due to the chemical energy production mechanisms. The idea of beamed energy propulsion was first put forward by Konstantin Tsiolkovsky[1] in 1924 and then later expanded on by Shad and Moriarty[2] who first proposed the concept of launching objects specifically with beamed microwave energy from a ground-based source. Since the work of Shad and Moriarty, a great deal of research has been done leading to a wide variety of beamed microwave propulsion concepts as well as significant advances in microwave generation.

Launch concepts based on beamed energy propulsion can fall into one of three categories: 1) direct energy coupling to the propellant, 2) energy addition to a heat exchanger, or 3) energy coupling via plasma formation. This analysis will look at directly coupling microwave energy to the effluents of a solid rocket motor in the diverging section of the nozzle. Through direct energy coupling, this concept involves augmenting the thrust of an existing rocket by first heating liquid alumina particles produced by the thruster, then transferring that energy to the expanding gas via gas-particle collisions. Simply augmenting the thrust of an existing rocket has several distinct advantages. First, since the microwave energy radiates from a remote, ground-based source, the mass increase on the vehicle itself is minimal. Second, only the diverging section of the nozzle would need altering to handle higher temperature operation since the power addition only occurs in this section. Finally, the enhanced performance, provided by this beamed propulsion concept, can lead to the reduction in the complexity of launch vehicle staging and possibly single stage to orbit operation. Thrust augmentation using beamed energy does have several drawbacks. First, microwave coupling to supersonic, two phase flow needs to be investigated. Next, the redesign of the nozzle is required to handle high temperature loads. Finally, because large power densities are required, the infrastructure cost of such a ground-based facility will be quite high.

The second of the aforementioned categories has been studied primarily by Parkin.[3] Through his research, he has developed a concept for a "Microwave Thermal Thruster" which involved beaming microwave power to a heat exchanger attached to the launch vehicle. The heat exchanger absorbs the energy and transfers it to a hydrogen propellant flowing through an array of small channels. Parkin et al. indicate that a hydrogen propellant is capable of producing 54 kN of thrust with a specific impulse of over 1000 seconds.[4] Parkin and Culick estimate that a one metric ton vehicle can carry 100 kg of payload to an 1100 km circular orbit using 275 MW of beamed energy.[5] This system offers the benefit of higher exhaust velocities over traditional chemical rockets and thus higher specific impulse.

Researchers at the University of Tokyo have investigated a concept utilizing beamed microwave energy to produce plasma near the focal point of the directed beam.[6,7] The formed plasma then absorbs the remaining microwave pulse to increase the enthalpy of the propellant. The vehicle utilizes repetitive pulses to induce plasma in either the stored propellant or the air to propel the vehicle. Both the systems proposed by the researchers at the University of Tokyo and Parkin et al. use the beamed power as the sole source of propulsive force. The concept in

this manuscript (where microwave augmentation merely enhances the vehicle performance) can be viewed a short term alternative to these aforementioned concepts. This could significantly reduce the risk of attempting to launch an initial beamed microwave vehicle while providing a technology demonstration for the concepts derived by other authors. Other advantages to the proposed concept include no mass increase due to a heat exchanger and no energy losses due to plasma formation.

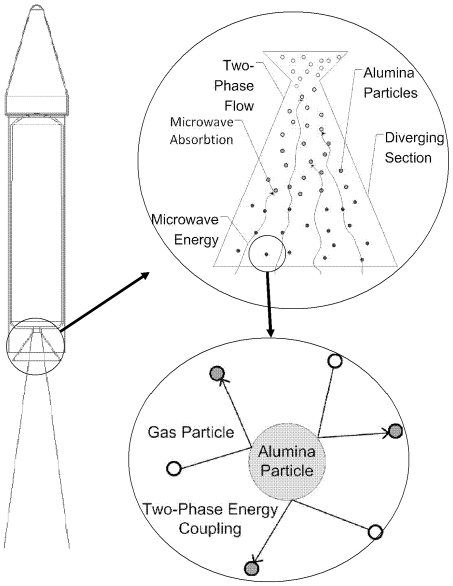

Figure 1. Microwave thrust augmentation through direct coupling to alumina particles.

In this study, the performance of a notional Castor 120™ is studied in both un-augmented and augmented scenarios. Although the Castor 120™ solid rocket motor is by no means optimized for a thrust augmentation application, it provides a baseline design with well quantified performance characteristics. The un-augmented mass and performance characteristics of the Castor 120™ are shown in Table 1.[8] In the augmented case, the Castor 120™ is augmented for the first 50 km of its vertical ascent. An altitude of 50 km was chosen based on potential beam propagation issues through the atmosphere beyond this altitude. In general, the augmentation (microwave energy addition) was assumed to bring the alumina particles in a Castor 120™ nozzle to their boiling point at 3200K. The critical analysis presented in this manuscript is two-fold. First, an experimental study is presented involving the microwave coupling efficiency of solid aluminum oxide (alumina) particles at room temperature with a 2.45 GHz microwave power source. Second, a numerical study is presented on the performance of the Castor 120 evaluating the gains of augmenting the thrust, as well as power requirements to obtain desired thrust augmentation factors.

Table 1. Castor 120 Characteristics.

Characteristic	Value	Characteristic	Value
Burn Time	79 s	Wet Mass	530,767 kg
Average Vacuum Thrust	1,687,655 N	Dry Mass	4071.5 kg
Maximum Vacuum Thrust	1,881,597 N	Propellant Mass	49,005.2 kg
Average Pressure	8.58 MPa	Mass flow rate	620.31 kg/s
Maximum Pressure	9.99 Mpa	Throat diameter	0.365 m
Specific Impulse	280.2 s	Exit diameter	1.52 m
Exit Velocity	2,000 m/s	Expansion Ratio	24

II. Microwave Coupling to Solid Alumina Particles

The process of coupling microwave energy to alumina particles in the solid rocket motors exhaust is paramount to assess the potential of this concept study. The thrust augmentation process can be achieved in one of two ways: 1) heating alumina droplets with microwave energy and transferring that energy to the expanding gas through

collisions, or 2) vaporizing the alumina droplets through the microwave energy and adding molecular species to the flow. Because of the relatively high latent heat of vaporization of alumina, vaporization is not expected to contribute to the overall augmentation process. Therefore, thrust augmentation will occur in a two step process. First, the alumina particles will be heated in the nozzle (through microwave addition) from their nominal combustion chamber temperature of approximately 2500 K to their boiling temperature of approximately 3250 K. Constant microwave energy addition will allow the particles to maintain a temperature of 3250 K throughout the nozzle. The particles then are used as a heat exchanger with the surrounding gas. Through gas-particle collisions, the gas enthalpy is increased. As the gas expands through the nozzle, it converts the imparted thermal energy to kinetic energy, thus increasing the thrust. This augmentation process is depicted in Fig. 1. For the purposes of this study, an experiment was conducted to investigate the coupling capability of alumina particles with microwave energy.

A. Experimental Setup

Results from Weber et al.[9] give an absorption coefficient for molten alumina in the visible wavelength range from 0.385 to 0.780 μm. Thostenson and Chou[10] investigate the effects of radiating ceramic powders in the microwave range. The purpose of this experiment is to generate a coupling efficiency for solid alumina particles at 2.45 GHz. To back out a coupling efficiency of microwave energy to alumina particles a comparison of the power of a 2.45 GHz system was done in relation to a standard plate heater to a steady state temperature. A sample of alumina power with an average particle size of 10 microns was radiated in a 0.23 m^3 Faraday cage with a 2.45 GHz magnetron. The temperature of the particles was read using an infrared pyrometer from outside the Faraday cage. A diagram of the experimental setup is shown in Fig. 2. First, a sample of 0.0775 kg of alumina particles was irradiated with the magnetron until they reached a steady state temperature. Temperature measurements were then taken a rate of 1 Hz for the period of one hour while measuring the forward and reflected powers of the microwave source. The alumina particles were then heated using an quartz faced panel heater to the same steady state temperature. The heater voltage was varied using a variable transformer and the power output from the heater was measured. The temperature was monitored using the same pyrometer setup as the microwave test at the same emissivity. To obtain the coupling coefficient for the alumina particles, the ratio of power from the heater to the power from the microwave system (at the same steady state temperature) was calculated.

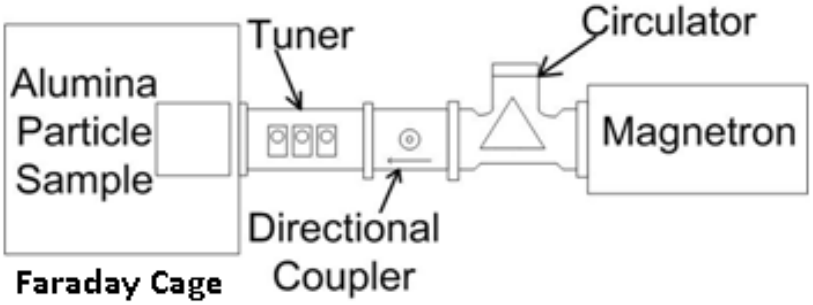

Figure 2. Experimental Setup.

B. Results

During the microwave test, the alumina powder reached a steady state temperature of approximately 543°C after a period of 42 minutes as shown in Fig. 3. The downstream microwave power level reaching the alumna powder during this test remained relatively constant at 1.811 kW. Within 10 seconds of full microwave power, the particles exhibited a rapid energy absorption as indicated in Fig. 3. The sample was then cooled and reheated using the plate heater to the same steady state temperature with an input power of 1.033 kW. Assuming that the losses by both the plate heater and the microwave systems are the same, the efficiency of microwave absorption by alumina particle was found to be 57.1% by taking the ratio of the input power by both heating techniques.

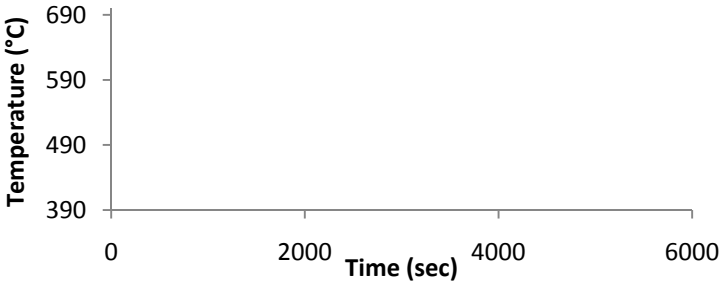

Figure 3. Pyrometer Temperature data for microwave irradiation of alumina particles.

In developing the coupling efficiency several assumptions were made. First, the losses due convection cooling and conduction through the Faraday cage were assumed to be the same for both the microwave and resistive heater configurations, and therefore were neglected in the calculations. Also, the emissivity of the sample was assumed to be constant through the heating process. The instrumentation in this experiment induced a certain amount of error in the power calculations. The microwave power meter has a resolution of 4 W and an accuracy error of 0.01% yielding a percent error of 0.1 %. The power measurements for the plate heater have errors of approximately 4%. The total coupling efficiency error due to instrumentation was approximately 2.2%.

III. Development Numerical Model for Two-Phase Flow with Energy Addition

A combined Eulerian-Lagrangian approach with a two-way coupling was used to model the impact of the microwave radiation on the two-phase flow inside the nozzle of a solid propellant thruster. Gas properties were computed using an Eulerian approach based on the solution of the Navier-Stokes equations with appropriate source terms that take into account the impact of particulates on the gas flow,

$$\frac{D\rho}{Dt} + \rho(\nabla \cdot \mathbf{V}) = 0,$$
$$\rho\frac{D\mathbf{V}}{Dt} - \nabla \cdot \mathbf{\Pi}_{ij} = D_i,$$
$$\rho\frac{D\mathbf{V}}{Dt} \cdot \mathbf{V} + \nabla p \cdot \mathbf{V} - (\nabla \cdot \tau_{ij}) \cdot \mathbf{V} = Q,$$

where

$$D_i = 3\pi d_{part} n_{part} \nu (1 + 0.15 * Re^{.687})(u_{pi} - u_{gi})$$

and

$$Q = 2\pi d_{part} n_{part} \lambda (1 + 0.3\sqrt{Re}) Pr^{1/3}$$

Here, Reynolds and Prandtl numbers are defined as

$$Re = \rho_g d_{part} |\vec{u}_p - \vec{u}_g| / \nu \text{ and } Pr = \nu C_{p_g} / \lambda.$$

The Navier-Stokes equations were solved using Versatile Advection Code (VAC)[11] modified to include the above particle source terms. Particle properties were determined by Lagrangian tracking of particles through the gas flowfield and statistical averaging of particle properties. Developed in this work Lagrangian particle tracker, combined with the Eulerian gas phase module (modified VAC) into a two-phase flow solver VAC-2P, was used to obtain two-phase flow solution through two successive steps. First, steady state solution of gas flow was computed, with the particle source terms set to zero. Then, alumina particles were introduced at the nozzle throat, with their surface temperature and velocities set to the corresponding gas temperature and velocities, and steady-state two-phase flow solution was computed. For the gas phase, an explicit time integration with CFL=0.4 was used, and the Navier-Stokes equations were solved using the TVD-Lax-Friedrichs scheme with minmod limiter. For the particle phase, a fourth order Adams-Moulton method was used to integrate particle equations of motion. Force on the particle was calculated as

$$F_i = 3\pi d_{part} \nu (1 + 0.15 * Re^{.687})(v_{pi} - u_{gi})$$

where the Reynolds number is based on the individual particle velocity. Particle temperature at the next step was determined as

$$\Delta T = \frac{12\Delta t(1+0.3\sqrt{Re}Pr^{1/3})\lambda_f}{C_{p_{part}}\widetilde{\rho_p}d_{part}^2}(T_g - T_{p_j}) + \frac{\Delta t 4\pi f \epsilon_m \tan\delta I}{cC_{p_{part}}\rho_{part}}$$

Different timesteps were used for the integration of the Navier-Stokes equations and particle tracking, with particle tracking timestep approximately an order of magnitude larger than the Eulerian stage timestep. Particle macroparameters (number density, temperature, velocity) used in the Eulerian source terms were determined by simple averaging over each cell.

IV. Two-Phase Flow Analysis

Consider first a two-phase flow through a CASTOR 120 type nozzle in the absence of any MW heating. Two CFD solvers are used for modeling of this flow, the VAC based solver VAC-2P discussed in the previous section, and a commercial software package CFD++[12] developed by Metacomp Technologies, Inc. Comparison of a new VAC-based two-phase capability with an established CFD solver provides basis for model comparison and accuracy analysis. CFD++ is a flexible computational fluid dynamics software suite for the solution of steady and unsteady, compressible and incompressible Navier-Stokes equations, including multi-species capability for perfect and reacting gases. In this work, a turbulent Reynolds Averaged Navier-Stokes capability of CFD++ is applied. The simulations were performed with axial symmetry, with a 2nd order in space algorithm, and a two equation k-epsilon turbulence model. Implicit time integration was used. A general multi-phase capability has been used that provides an Eulerian description of the disperse phase (particulates).

For both flow solvers, the computations presented below were performed for a single-block rectangular grid with a total of 7,200 nodes, that covers the diverging part of the nozzle and the plume flow in the vicinity of the nozzle. Preliminary analysis with CFD++ has shown that the impact of the combustion chamber and the converging part of the nozzle on the flow in the diverging part of the nozzle and at the nozzle exit is relatively small, and therefore only the diverging part of the nozzle is considered below. The uniform boundary conditions were applied at the nozzle throat, with gas density, velocity, and temperature of 3.54 kg/m^3, 1019 m/s, and 2500 K, respectively. Supersonic outflow boundary condition was used at the nozzle exit plane, and the adiabatic condition was prescribed at the wall. To simplify the analysis, a single effective perfect gas species and a single alumina particle diameter of 4 micron were considered in the simulations. The particle mass loading of 32% was specified at the nozzle throat, and particle temperature and velocity at the throat were assumed to coincide with the corresponding gas properties.

The gas temperature and particle surface temperature obtained with two flow solvers are presented in Fig. 4. Note that the transient heat conduction inside the particles is not considered, and particles are assumed to have a single material temperature (surface temperature, or simply temperature hereafter). Comparison of the two solutions show good agreement between gas temperatures in the first half of the nozzle, whereas there is a visible difference between the solutions in the second half of the nozzle and in the plume. At the nozzle exit, the gas temperature obtained by VAC-2P is over 100 K higher. The particle temperature at the exit plane is somewhat lower than in CFD++. Note also the difference between the particle temperatures in the first half of the nozzle, with VAC-2P solution being lower. Excellent agreement between gas-only solutions, obtained in preliminary studies, allows the authors to attribute the differences between the two solutions to the differences in the particle-gas heat transfer and drag models used in the two solvers. There is obviously a stronger heat transfer coupling between alumina particles and gas flow in VAC-2P than in CFD++. Note that the observed differences in the solutions, although noticeable, are significantly smaller than those obtained earlier between three commercial codes CFD++, Fluent, and CFD-Ace.[13]

Let us now compare the gas and particle temperature fields computed with VAC-2P. The gas temperature decreases quickly from 2500 K at the nozzle throat to about 1500 K at the nozzle exit. The maximum temperature along the nozzle exit plane is observed off the nozzle axis due to the formation of the boundary layer. It is clearly seen that the boundary layer occupies relatively small part of the nozzle. The rapid gas expansion and cooling results in significant decrease of the particle surface temperature inside the nozzle. For the flow conditions inside the nozzle, the gas density is high enough for the gas-to-particle heat transfer to be dominant, and the gas and particle temperatures are close. As gas expands, and the density decreases, the particle drag force is also decreases, and the difference between the particle and gas temperatures becomes visible, increasing from a few degrees near the nozzle throat to about 30 K in the plume. In the coreflow at the nozzle exit plane the particle temperature is about 20 K higher than the gas temperature. Near the wall this difference is smaller, and amounts to less than 10 K. The important conclusion from the analysis of the temperature fields is that heat transfer coupling between gas and

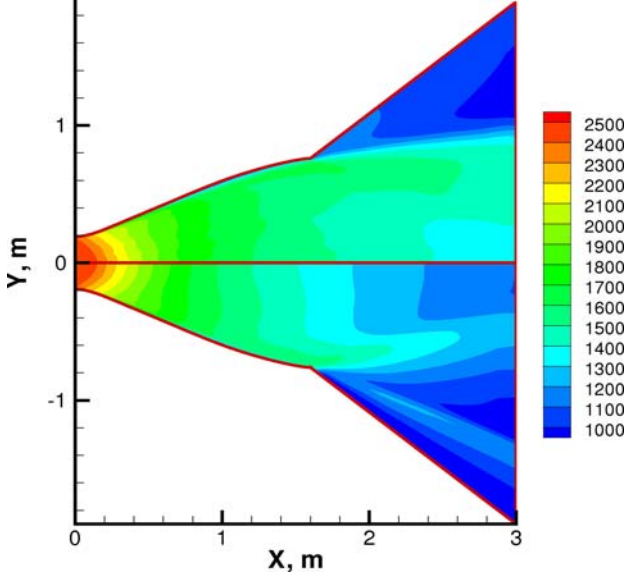

Figure 4a. Gas temperature (K) for the no MW radiation case.

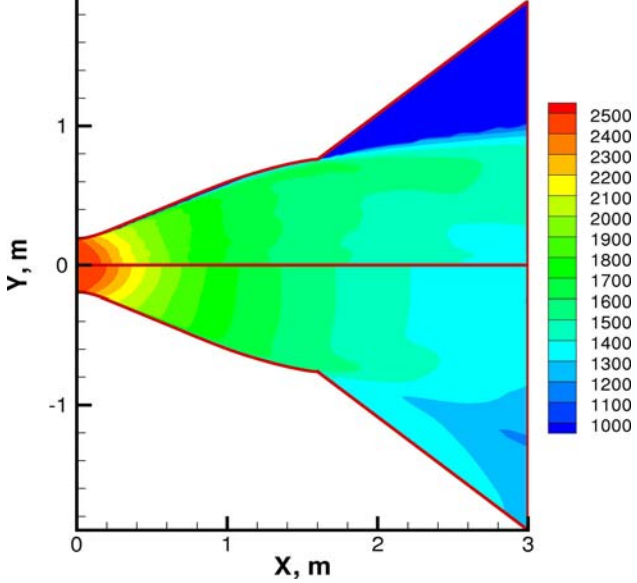

Figure 4b. Alumina particle temperature (K) for the no MW radiation case.

particles in a CASTOR 120 motor is high enough for any change in particle temperature due to microwave heating to be immediately transferred to gas. That means that even though the gas is not significantly heated when exposed to the MW radiation, alumina particle heating may be a robust mechanism for increase in gas enthalpy.

Second most important parameter, in addition to gas temperature, is gas velocity, since increasing gas velocity at the nozzle exit through the microwave heating is the main goal of the MW energy deposition. The gas and particle axial velocity fields obtained with the two approaches are shown in Fig 5a and 5b, respectively. The two solutions are very similar in the first half of the nozzle. Then, there are somewhat smaller gas and particle velocities near the nozzle exit and in the plume for the VAC-2P solution. This is explained by slower rate of heat exchange between gas and alumina particles in CFD++, shown in Fig. 4, and thus faster gas cooling and transfer from thermal to kinetic gas energy. Note that VAC-2P solution predicts no particles in the plume for angles larger than the nozzle exit angle (particles are too heavy to be turned at larger angles).The particle velocities are undefined in that region. In CFD++, which uses an Eulerian description of particulates, there is still some small fraction of particulates, which have very high velocities of over 2400 m/s, but they are of numerical and not physical origin.

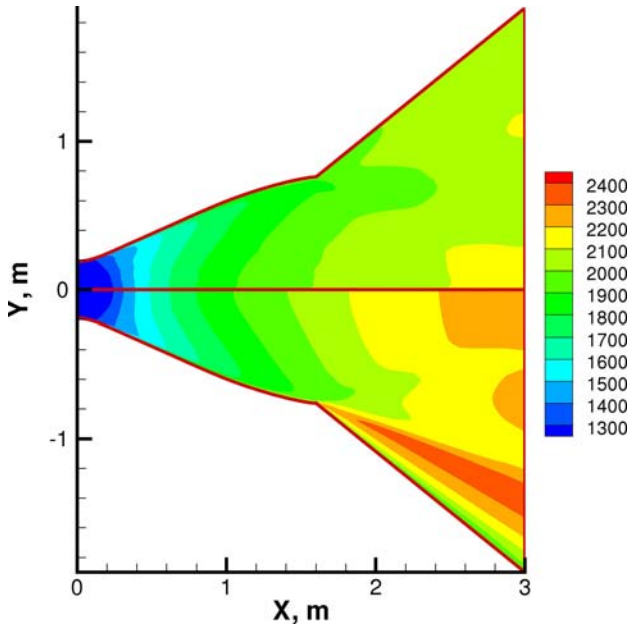

Figure 5a. Gas axial velocity (m/s) for the no MW radiation case.

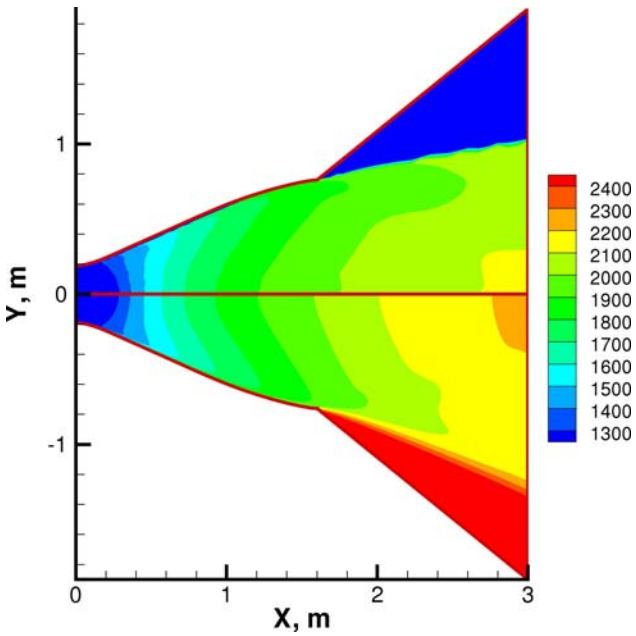

Figure 5b. Particle axial velocity (m/s) for the no MW radiation case.

Analysis of VAC-2P solution shows that the velocity increase is most significant in the first third of the diverging part, where it increases by approximately a factor of two to about 1500 m/s. In the last third of the nozzle

the increase is relatively small, only about 100 m/s. The gas exit velocity near the nozzle axis is about 2000 m/s. The position of the boundary layer is clearly seen; at the nozzle exit plane its thickness is slightly more than 10% of the nozzle exit radius. The alumina particle axial velocity field is qualitatively and quantitatively very similar to that of the gas. At the nozzle exit plane, it is only about 30 m/s lower than the gas velocity, which amounts to 1.5% of the total velocity magnitude. This indicates that the drag force is very significant inside the nozzle, and the increase in gas velocity due to enthalpy addition to the flow will be accompanied by similar increase in particle velocity. In terms of the MW - particle interaction, this may result in a considerable reduction of the interaction time for a given nozzle geometry.

V. Physical Mechanisms of the MW / Two-Phase Fluid Coupling

The immediate effect of the interaction of microwave radiation with the two-phase flow inside the diverging part of a solid propellant thruster is expected to be an increase of alumina particle temperature. This in turn will result in an increase in gas temperature and then gas and particle velocities. The schematics of such an interaction is shown in Fig. 6. It is clear that the ability of the microwave radiation to considerably improve the performance of a thruster through the interaction with the expanding flow greatly depends on flow parameters in the diverging part of the nozzle. The coupling of the radiation with a two-phase flow in a solid propellant engine is mostly determined by the properties of the alumina particles that are expected to dominate the radiation-to-media heat transfer in the absence of significant gas ionization. The macroparameters of alumina particles, such as their temperature, size distribution, and number density, influence the amount of radiation being absorbed by the media. The performance of the thruster impacted by the microwave radiation strongly depends on the feedback from the gas, the impact of the walls, and the fact that much of the radiation is expected to be absorbed as the photons travel upstream in the diverging part of the nozzle.

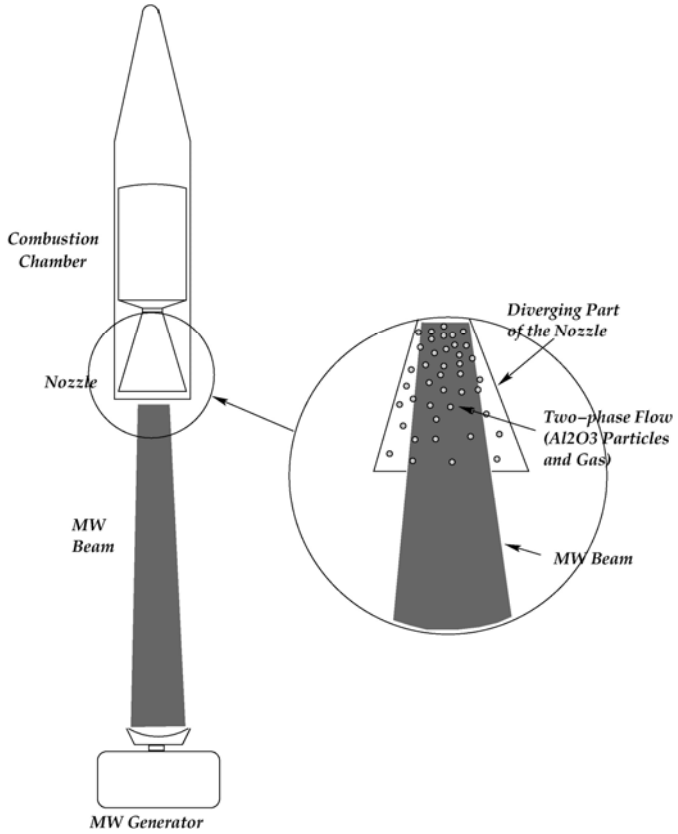

Figure 6. Schematics of the MW beam - nozzle flow interaction setup.

Generally, two important issues need to be considered that impact the thruster performance increase due to the energy deposition from MW radiation to alumina particles inside the nozzle. First is related to the possibility of MW

photons to heat particles fast enough to sufficiently high temperatures, and the second is associated with the efficient transfer of internal energy of particles to gas and then successive conversion of the gas molecule thermal motion to the directional motion along the nozzle axis. The above numerical analysis shows the possibility to effectively transfer heat from particle surface to gas inside the diverging part of the nozzle under consideration. The first issue is, however, more difficult to estimate. The rate of the heating of a particle exposed to the MW radiation may be expressed as the corresponding temperature rise ΔT in a time interval t, and written as (see, for example, Ref. 14),

$$\Delta T = \frac{\omega \varepsilon_0 \varepsilon' \tan(\delta) |E^2|}{\rho C} t.$$

While the material properties of alumina are reasonably well known, and the electric field properties are given for every particular MW generator setup, the alumina optical properties at very high temperatures are not known. The authors are not aware of any experimental data where the MW energy dissipation in alumina would be measured at temperatures in the range from 2,300 K to 3,000 K, although there is a significant number of papers devoted to the low-temperature alumina optical properties (see, for example, Ref. 15). The situation is complicated by the fact that there are several alumina phases present in the exhaust, from the liquid alumina for temperatures higher than the alumina melting temperature of 2,325 K to γ alumina at lower temperatures to α alumina, with partially melted particles also being present in large numbers. Different phases are expected to have different optical properties in the microwave range, similar to the properties at wavelengths known from experimental studies, such as those in the UV and IR bands. Another difficulty is related to the impurities inherent in alumina particles in the exhaust. Even though the impurities may amount to less than 1% of the total particle mass, they may still significantly change (and generally increase) the MW energy dissipation.[16]

Experimental studies of a 92% pure α alumina have been conducted,[17,18] and the dielectric loss factor $\varepsilon' \tan(\delta)$ has been measured for temperatures from about 300 K to 2,100 K at 6 GHz. It is interesting to note that starting from approximately 600K, the loss factor increases exponentially, from below 0.01 to more than 1 at 2,100 K. Extrapolation of the exponential dependence to the alumina particle temperatures at the nozzle throat gives the loss factor of about 10. The analysis of the alumina optical properties of different purities for temperatures up to about 1,600 K, based on existing experimental data, was conducted in Ref.16. The relative dielectric constant ε' is a relatively week function of temperature, increasing for 99% pure alumina from 9.5 at room temperature to approximately 11 at 1,600K. The loss tangent, however, strongly increases with temperature. At a temperature of 1,600 K it amounts to about 0.01 for a 97% pure alumina and 0.004 for 99% pure alumina, which results in a loss factor of about 0.1 and 0.04, respectively. Assuming an exponential dependence of the loss factor on temperature, and extrapolating it to higher temperatures, one may expect to have the loss factor on the order of 10 for the flow conditions near the nozzle throat. The value of 10 therefore has been used in this work. The effective life time of particles in the diverging part of the nozzle may be estimated at approximately 1 ms, and for a 10 GHz beam and the electric field intensity of 1 GW/m^2, one can calculate the average increase in particle temperature well in excess of 2,000 K. This is a clear indication that the alumina particles may be heated quickly inside the nozzle and maintained at their boiling temperature of 3,250 K. Note that no significant alumina vaporization is expected due to an extremely high vaporization heat of 1.9×10^6 J/mol.

VI. Microwave / Two-Phase Nozzle Flow Coupling

The high thermal and velocity coupling between the gas and particulate phases in a CASTOR 120 nozzle flow shown in the previous section enables an efficient transfer of radiation energy from an incoming microwave beam to thermal and then kinetic gas energy. The results presented below are obtained with VAC-2P via a one-way coupling of a MW beam entering the nozzle and a two-phase flow with parameters and models used in the previous section. The microwave beam is assumed to enter the nozzle from the nozzle exit plane and then propagate upstream to the nozzle throat. Two constant microwave intensities are considered here, 100 MW/m^2 and 1GW/m^2.

The particle and gas temperature fields are presented in Fig. 7 for three cases, (i) no microwave beam, (ii) 100 MW/m^2, and (iii) 1GW/m^2. Comparing the first two cases, it is clear that the interaction between the MW radiation and alumina particles causes a noticeable increase in particle temperatures (Fig. 7a). The difference between particle temperatures in these two cases increases as the flow moves along the nozzle, reaching its maximum of about 250 K near the nozzle exit plane. The increase is practically the same in the coreflow and near the nozzle surface. The higher microwave intensity of 1 GW/m^2 is characterized by significantly larger amount of MW energy transferred to the particle internal energies. The particle temperature in case (iii) increases from its throat value of 2500 K to over

3200 K in the first half of the nozzle, and stays nearly constant through the second half of the nozzle. The particle temperature there is a few degrees colder than the boiling temperature since there is an energy transfer from particle internal modes to gas translational modes and finally to the particle translational modes. The particle surface temperature quickly decreases in the plume where the MW energy is not deposited.

The gas temperature fields for the three cases under consideration, shown in Fig. 7b, illustrate strong coupling between the particle internal energies and the gas translational energies. In all cases, the gas translational temperature is only slightly smaller than the corresponding particle surface temperatures. For case (iii), the gas temperature at the nozzle exit plane is about 3160 K, which is about 90 K lower than the particle boiling temperature of 3250 K. Note here that the value of the boiling temperature used in this work is that of α alumina. The boiling temperature of γ alumina is higher, although the actual boiling temperature depends on the amount of liquid and solid phases in each particle, which in turn is a function of particle size and surrounding gas properties. The value of 3250 K may be considered as the lower limit of the actual boiling temperature. It is interesting to note that near the plume axis at X=2.5 m, the gas temperature is a few degrees higher than the particle temperature, which is explained by the difference in particle and gas velocities. The particle-gas drag force decreases the difference between these velocities and results in some gas and particle heating; obviously, the gas heating is more efficient than the particle heating.

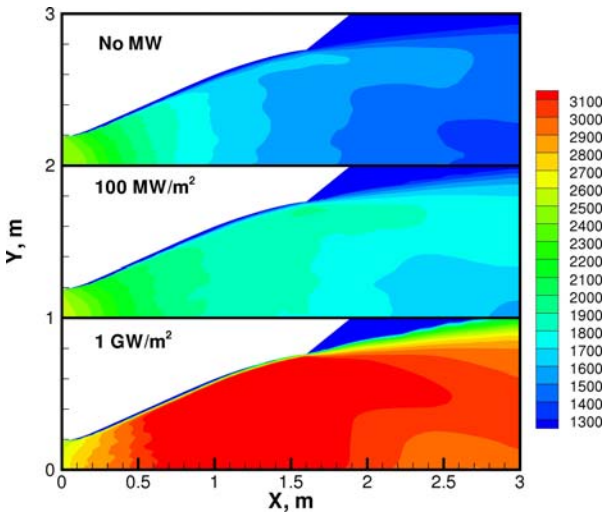

Figure 7a. Particle temperature (K) for different MW intensities.

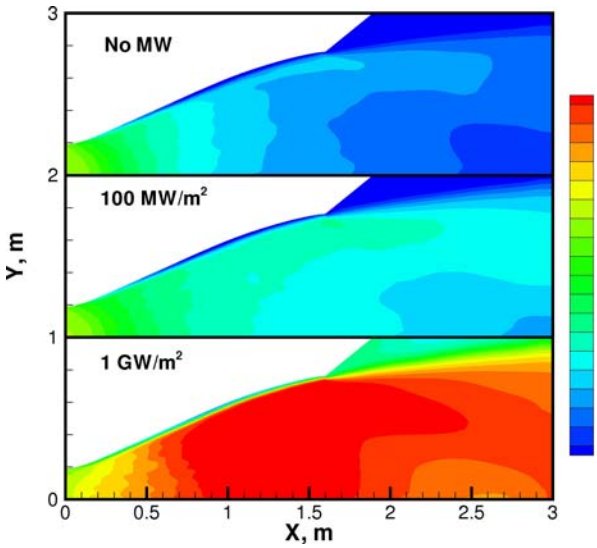

Figure 7b. Gas temperature (K) for different MW intensities.

The impact of the MW beam / alumina particle coupling on gas velocities in the axial direction is shown in Fig. 8a. As expected, the presence of the radiation has smaller effect on gas velocities than on gas and particle temperatures. The gas velocity at the nozzle exit increases for case (ii) by about 1% as compared to the no radiation case. For case (iii) it increases by approximately 9% in the coreflow and about 6% near the nozzle lip. The MW energy deposition has also some effect on gas densities, as illustrated in Fig. 8b. It slightly improves flow directionality in case (iii), where a smaller difference between the gas density in the coreflow and near the nozzle surface is observed. Near the nozzle axis, the gas density at the nozzle exit plane is about 7% higher for case (iii). Near the nozzle lip, it is up to 25% lower. The computed thrust increases from 0.989 MN for case (i) to 1 MN for case (ii) to 1.13 MN for case (iii). The latter value is only slightly smaller than the thrust value of 1.14 MN, computed for a constant particle temperature of 3250 K.

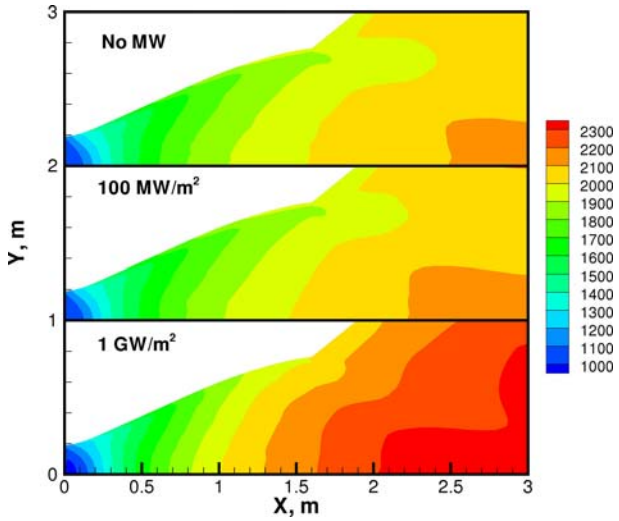

Figure 8a. Gas axial velocity (m/s) for different MW intensities.

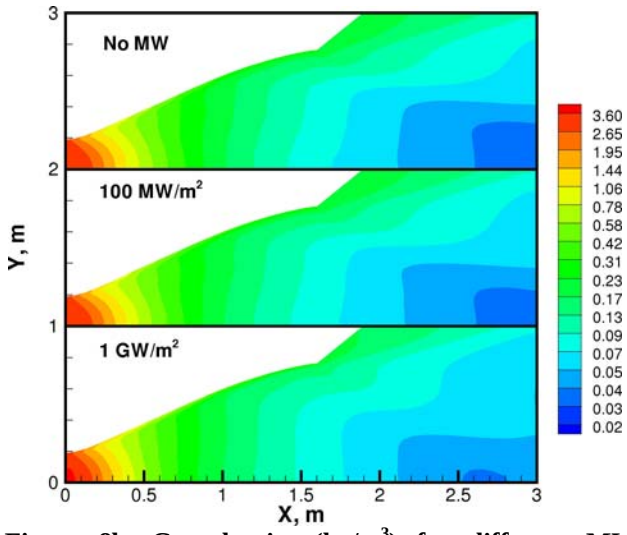

Figure 8b. Gas density (kg/m^3) for different MW intensities.

VII. Upper Limit for the Thrust Increase

The above analysis shows that for high enough intensities of the microwave beam (larger than 1 GW/m^2), the following assumptions may generally be made, (i) the alumina particles are quickly heated to their boiling temperature near the nozzle throat, and then kept at that temperature as they move to the nozzle exit, and (ii) the gas-particles heat transfer is very fast, so that the gas comes to thermal equilibrium with particles over distances much smaller than the length of the diverging part of the nozzle. The second assumption seems reasonable for a CASTOR 120 type motor, based on the numerical results presented earlier, while the first assumption does require very large MW intensities to be applied. With the above assumptions, the expansion of gas in the diverging part of the nozzle is affected by a heat source (alumina particles) that keeps the gas at a boiling temperature of aluminum. This may be simplified to consider it as an expansion of a gas with a very large number of internal degrees of freedom. The latter implies a gas with the specific heat ratio γ that tends to the unity. Since the boundary layer in a CASTOR 120 nozzle is relatively thin (about 10% of the nozzle exit diameter at the exit plane), one can use one-dimensional isentropic expansion relations to write the upper estimate for the Mach number at the nozzle exit as

$$\lim_{\gamma\to\infty}\left(\frac{\gamma+1}{2}\right)^{-\frac{\gamma+1}{2(\gamma-1)}}\left(1+\frac{\gamma-1}{2}M^2\right)^{-\frac{\gamma+1}{2(\gamma-1)}}\frac{1}{M}=\frac{A_e}{A_t}$$

Here, A_e and A_t are the exit and throat areas, respectively. This expression may be reduced to

$$\frac{\sqrt{\exp\left(M^2\right)}}{eM^2}=\left(\frac{A_e}{A_t}\right)^2$$

For a CASTOR 120 nozzle, the exit Mach number is about 3. Since the expansion ratio for this nozzle is 24, the maximum Mach number that can possibly be reached at the nozzle exit, as estimated from the above relation, is about 4.5. This is about 50% higher than the Mach number at the exit of the actual Castor 120 motor. The total thrust increase should also be about 50%. Obviously, this is the upper limit for the efficiency increase of a CASTOR 120 thruster, and it is significantly larger than a ~15% increase obtained earlier with VAC-2P code. Note that changing the design of the nozzle or choosing different propellant may increase the computed thrust, but such a study was out of the scope of this work.

VIII. Conclusion

Feasibility of using a high intensity microwave beam to increase thrust of a solid propellant motor over the first part of the launch trajectory through the deposition of the radiation energy into the internal energy of alumina

particles in the diverging part of the nozzle has been studied. A CASTOR 120 motor was considered as an example of a high thrust launch motor, and two MW intensities have been considered, 100 MW/m^2 and $1GW/m^2$. In the high-density environment of a CASTOR 120 type motor, microwave energy was found to be transferred effectively to the internal energy of alumina particles and then to gas and particle kinetic energies, thus increasing the total thrust. The increase in the total thrust was about 14% for the $1GW/m^2$ case. The total power increase is about 20%, which indicates that nearly all microwave energy may be transferred to the kinetic energy of the expanding flow.

Acknowledgments

The work was supported by the Advanced Concepts Group at the Air Force Research Laboratory, Propulsion Directorate, Edwards AFB, CA. The authors wish to thank Mr. Barry Cornella and Mr. Sean Hammerland for their assistance with the experimental portion of this work.

References

1. Tsiolkovsky(1924). *Spaceship*, 1924, in Izbrannye Trudy, Compiled by Vorob'ev, B.N., Sokol'skii V.N., General Editor Acad. Blagonravov, Izdatel'stvo Akademii Nauk SSSR, Moscow, Russia, 1962, 222 (in Russian). Edited Machine Translation prepared by Translation Division, Foreign Technology Division, WPAFB, Ohio, on May 5th, 1966, 307.
2. Shad, J. L., and Moriarty, J. J., "Microwave Rocket Concept," in XVI International Astronautical Congress, Athens, 1965.
3. Parkin, K. G., "The Microwave Thermal Thruster and its Application to the Launch Problem," Ph.D. Dissertation, California Institute of Technology, Pasadena, CA, 2006.
4. Parkin, K. G., DiDomenico, L. D., and Culick, F., "The Microwave Thermal Thruster Concept," *Proceedings of the Second International Symposium: Beamed Energy Propulsion*, ed. K. Komurasaki, AIP Conference Proceedings 702, Melville, NY, 2004, pp. 418-429.
5. Parkin, K. G., and Culick, F., "Feasibility and Performance of the Microwave Thermal Rocket Launcher," *Proceedings of the Second International Symposium: Beamed Energy Propulsion*, ed. K. Komurasaki, AIP Conference Proceedings 702, Melville, NY, 2004, pp. 407-417.
6. Oda, Y., Komurasaki, K., Takahashi, K., Kasugai, A., and Sakamoto, K., "Plasma Generation Using High-Power Millimeter-Wave Beam and Its Application for Thrust Generation," *J. Appl. Phys.*, Vol. 100, 113307, 2006.
7. Nakagawa, T., Yorichika, M., Komurasaki, K., Takahashi, K., Sakamoto, K., and Tsuyoski, I., "Propulsive Impulse Measurement of a Microwave-Boosted Vehicle in the Atmosphere," *J. Spacecraft and Rockets*, Vol. 41, No. 1, pp. 151-153, 2004.
8. Hilden, J., and Poirier, B., "Castor 120™ Motor:Development and Qualification Testing Results," *AIAA Paper 93-4277, AIAA Space Programs and Technologies Conference and Exhibits*, Huntsville, AL, September 1993.
9. Weber, J. K., Krishnan, S., Anderson, C., and Nordine, P., "Spectral Absorption Coefficient of Molten Aluminum Oxide from 0.385 to 0.780 μm," *Journal of American Ceramics Society*, Vol. 78, No. 3, March 1995, pp. 583-587.
10. Thostenson, E. T., and Chow, T. W., "Microwave Processing: Fundamentals and Applications," *Composites: Part A*, Elsevier Science Ltd., February 1999, pp. 1055-1071.
11. Toth, G. "General Code for Modeling MHD flows on Parallel Computers: Versatile Advection Code," Astrophysical Letters and Communications, Vol. 34, 1997, pp. 245-250.
12. Chakravarthy, S., and Peroomian, O., "Some Internal Flow Applications of a Unified-Grid CFD Methodology," AIAA Paper 96-2926, 32nd AIAA /ASME /SAE /ASEE Joint Propulsion Conference and Exhibit, Lake Buena Vista, FL, July 1996.
13. Gimelshein, S., Markelov, G., and Muylaert, J. Numerical Modeling of Low Thrust Solid Propellant Nozzles at High Altitudes , AIAA-2006-3273, 37th AIAA Plasmadynamics and Lasers Conference, San Francisco, California, June 5-8, 2006.
14. Mingos, D.M.P., "Theoretical aspects of microwave dielectric heating," *Microwave Assisted Organic Synthesis*, ed. by J.P. Thierney and P. Lindstrom, Blackwell Publishing, 2000, pp. 1-21.
15. Braginsky, V.B., Ilchenko, V.S., Bagdassarov, Kh.S., Experimental observation of fundamental microwave absorption in high-quality dielectric crystals, *Phys. Letters A*, Vol. 120, No. 6, 1987, pp. 300-306.
16. Sutton, W.H., "Microwave processing of ceramic materials," *Ceramic Bull*., Vol. 68, No. 2, 1989, pp. 376-386.
17. Fukushima, H., Yamanaka, T., Matsui, M., "Measurement of Dielectric. Properties of Ceramics at Microwave Frequency," *J. Japan Soc. of Prec. Eng.*, Vol. 53, 1987, pp. 743-748.
18. Fukushima, H., Yamanaka, T., Matsui, M., "Microwave heating of ceramics and its application to joining," *J. Mater. Res.*, Vol. 5, No. 2, 1990, pp. 397-405.